STU
SLOVAK UNIVERSITY OF TECHNOLOGY IN BRATISLAVA

Journal of Electrical Engineering, Vol. 76, No. 6, 2025, pp. 574-585
https://reference-global.com/journal/JEE

Numerical and experimental investigation of PZT droplet ejection under pulsed voltage for electrohydrodynamic printing

Xue Yang[1], Mingchao Bi[2], Zhifu Yin[3,4], Xiao Xu[5]

Lead zirconate titanate (PZT) has grown increasingly crucial for micro-electro-mechanical systems (MEMS) sensors, including accelerometers, vibration sensors, ultrasonic transducers, and wearable electronic devices. However, most existing fabrication methods face limitations such as incompatibility with traditional MEMS processes and high manufacturing costs. On-demand electrohydrodynamic (EHD) printing enables the low-cost fabrication of micro- and nano-scale PZT structures without the need for a mask. Unlike previous EHD printing techniques that use direct current (DC), this study proposes a PZT EHD printing method employing pulsed voltages, which offers greater flexibility. We developed a simulation model to analyze the formation of droplets under high-voltage pulses, demonstrating the droplet formation mechanisms in both dripping and jetting modes, as well as the accompanying satellite droplet phenomenon. Additionally, we investigated the effects of printing parameters and ink properties on the size of ejected droplets. Results from PZT EHD printing experiments and practical applications confirm that our proposed printing method holds significant potential for the subsequent fabrication of various MEMS PZT sensors.

Keywords: electrohydrodynamic jet printing, piezoelectric ceramic transducer, pulsed voltage, droplet ejection, numerical simulation

1 Introduction

Lead zirconate titanate (PZT)-based micro-electro-mechanical systems (MEMS) sensors with membrane structures are of great significance for detecting ultra-small acceleration, vibration, strain, and stress. This is primarily attributed to their exceptional sensitivity, high piezoelectric constant, and excellent electromechanical coupling coefficient [1]. Conventional methods for depositing PZT films include sputtering [2], chemical vapor deposition [3], bulk PZT bonding [4], screen printing [5], and aerosol deposition [6, 7]. Among these techniques, sputtering and chemical vapor deposition offer high fabrication precision but suffer from inherent limitations such as high costs and prolonged processing times. In contrast, bulk bonding, screen printing, and aerosol deposition are relatively simple and cost-effective. However, they lack the capability to fabricate fine-scale structures – a critical drawback that restricts their application in the manufacturing of MEMS PZT sensors.

Recently, direct writing technologies have been widely used for micro- and nano-scale functional structures, that they are always with low cost, simplified procedures, and low pollution [8]. By the direct writing method, we could fabricate patterns without using masking and etching processes. Inkjet printing, one of the direct writing approaches, has been developed for several decades, and it works by the generation of one-by-one droplets [9]. However, due to the surface tension of the ink drop, the droplet size we get on the substrate is always larger than the nozzle diameter. In other words, to produce micro-structures, we need a micro- or even sub-micro nozzle. It's obviously difficult to produce and manufacture such small nozzles. Besides, serious blockage problems would happen in narrow-sized nozzles during inkjet printing. To overcome the limitations of traditional inkjet printing, many studies have started exploring the potential of EHD (electro-hydrodynamic) printing, by which we can fabricate micro- and nano-scale patterns with large nozzles. This method utilizes an electric field between the nozzle and the substrate forming an electric field force to pull out the droplets. Under a high electric field, there is accumulation of charges at the interface of liquid and air. Then, a liquid cone is formed with the balance of liquid pressure, surface tension, and electrical stress. As a result, a micro- and nano-scale droplets could be generated at the apex of the nozzle. In this way, EHD

[1] School of Civil Engineering, Jilin Jianzhu University, Changchun, 130118 China
[2] The First Bethune Hospital, Jilin University, Changchun, 130021 China
[3] Guangxi Key Laboratory of Automatic Detecting Technology and Instruments, Guilin University of Electronic Technology, Guilin, 541004 China
[4] The State Key Laboratory of Refractories and Metallurgy, Wuhan University of Science and Technology, Wuhan, 430081 China
[5] Intelligent Centralized Control Center, Jilin Oilfield New Energy Company, Songyuan, 138000 China
yangx@jlju.edu.cn, bmc1988310@jlu.edu.cn, yinzf@jlu.edu.cn

https://doi.org/10.2478/jee-2025-0060, Print (till 2015) ISSN 1335-3632, On-line ISSN 1339-309X

printing could generate droplets/jets that are significantly smaller than the nozzle size (1/100 to 1/10 times) [10]. As EHD printing could write micro-/nano-patterned structures and micro/nanowires, it has been applied in the fields of flexible electronics [11], biological tissue engineering [12], flexible sensors [13, 14], and so on. It should be noted that inkjet printing retains irreplaceable value in large-area, low-precision manufacturing scenarios due to its high efficiency. The pulsed-voltage EHD printing proposed in this study is not intended to replace inkjet printing; instead, it provides a complementary, low-cost, mask-free fabrication solution tailored to the demand for micro/nano-scale fine structures in MEMS PZT sensors.

EHD printing is a typical technique that is affected by coupled multi-physic [15]. It has been confirmed that applied voltage, flow rate, and printing distance are the main factors that decide jet modes. To realize the stable cone-jet mode, high applied voltage is needed, because high applied voltage could generate a sufficiently high tangential electric stress to maintain the backflow. However, extremely high voltage can lead to multi-jet mode. Meanwhile, low flow rate and high printing distance can also result in unstable and inefficient jet mode. Besides them, the physical properties of ink (viscosity, permittivity, and density) and the environmental characteristics (temperature and humidity of air) can influence the stability and resolution of EHD printing. By optimizing all the influence factors of EHD printing, we could get desirable resolution and stable jet mode.

The phenomena of the cone-jet mode have been extensively studied around the world. Calvo established a formula against jet shape, charge distribution, current, and flow rate in the cone-jet mode through a lot of experiments and observations [16]. Park reported a micro-capillary nozzle for jet printing of patterns and functional devices with micrometer resolution [17]. Li reported a nozzle with an inserted non-conductive fiber eliminated backflow, which made it possible to maintain the backflow without a more intense tangential electric stress [18]. The inserted non-conductive fiber helped reduce the required potential and allowed only the electric field to accelerate the liquid. All of their studies are about printing nozzles, so we could know that nozzles can widely influence the effectiveness of EHD printing. Paine proposed a drop-on-demand method by controlling stable oscillations in an unforced electrospray [19]. With the development of numerical methods, many scholars started to write calculation algorithms or utilize commercial software to analyze the process of jet printing. Lastow performed a two-dimensional simulation using the commercial software package CFX 4.4 without taking into account the electrical current in the system [20]. Using this method, the circulatory feature of the flow inside the Taylor cone was reproduced. Wu et al. simulated the process of cone jet formation and studied how the nozzle parameters influence the jet mode [21]. Through simulations and experiments, Robert learned a comprehensive mechanism of cone formation, jet emission, and break-up, and the liquid was treated as a Taylor-Melcher leaky dielectric model [22]. Collins presented that electrospray droplets are coulombically stable at the instant and found the existence of scaling law for droplet charge [23]. There are a good many publications studying the droplet generation process of EHD printing and the main factors influencing the process by simulations.

The above studies demonstrate that jet flow and droplets can be generated according to the applied voltage. Under DC (Direct Current) voltage jet flow could form, while under AC (Alternating Current) voltage droplets can be generated. Compared with DC voltage, AC voltage allows point-to-point on-demand printing and three-dimensional nano-structure deposition. Thus, complicated patterns and structures can be produced by using AC voltage. However, to the best of our knowledge, there are no simulation works studying the EHD printing process with AC voltage. It is critical to study the droplet generation process under AC voltage and analyze the main influencing factors including applied voltage, flow rate, duty ratio, and physical properties of ink (surface tension, conductivity, dielectric constant, density, and viscosity) systematically.

In this paper, a numerical simulation model was established to study the formation process of PZT droplets under pulsed voltage (AC voltage). The relationship between droplet size and main influencing factors, containing printing conditions and ink physical properties, was investigated based on an established model. Using the proposed simulation method, process parameters and physical properties of the ink could be optimized to form much smaller PZT droplets, and it is beneficial to control the EHD printing process and obtain high printing resolution.

2 Simulation and experimental details

2.1 Theoretical modeling and numerical methods

All numerical simulations were conducted using COMSOL Multiphysics 5.4 (COMSOL Inc., Burlington, MA, USA) – a finite element analysis soft-ware widely validated for addressing multiphysics coupling problems. To model the EHD printing process, three built-in physics modules within COMSOL Multiphysics 5.4 were integrated, specifically the Laminar Flow Module, Electrostatics Module, and Level Set Module. Figure 1 shows a schematic illustration of the EHD printing process, while the inserted view illustrates the computational domain and its boundary conditions for

numerical simulation. The computational domain was meshed using triquetrous elements, and finer grids were adopted in the center and at the interface between air and ink. The nozzle is filled with ink. The Inlet boundary (green label in Fig. 1) is designed to supply PZT ink into the stainless-steel nozzle at a controlled flow rate – consistent with the experimental ink delivery via the syringe pump (Section 2.2) – and this ink supply directly facilitates droplet ejection from the nozzle tip. The boundary labeled Outlet in the computational domain, represented by the blue label in Fig. 1, serves as the surface where ejected PZT droplets are deposited. The substrate is grounded (matching the experimental setup) to form a closed electric field loop with the voltage-applied nozzle. In the numerical model, its boundary conditions are defined as follows: fixed potential 0 V in the Electrostatics Module, and a 'no-slip' condition for the ink in the Laminar Flow Module – ensuring full consistency with the physical experimental configuration.

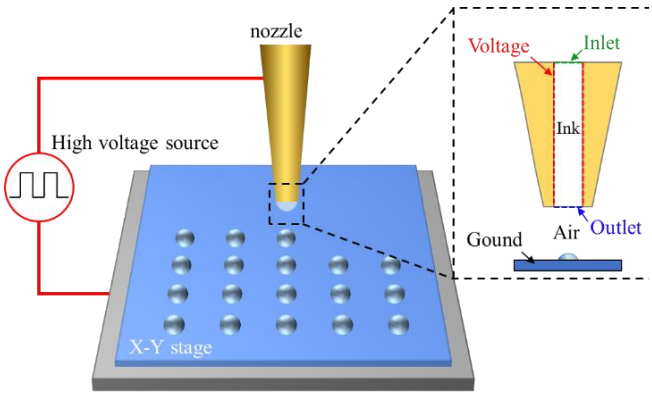

Fig. 1. The computational domain used for numerical simulation

Notably, the ink flow rate in the 2D numerical simulation is defined as the cross-sectional average velocity (m/s) applied at the 'Inlet' boundary, which is a common simplification for 2D axisymmetric models of EHD printing [24, 25]. This 2D velocity is derived from the experimental 3D volume flow rate by normalizing with the nozzle's cross-sectional area (calculated from the inner diameter listed in Tab. 1), ensuring consistency between simulation and experimental ink supply rates.

2.2. Experimental setup and PZT ink

In the present work, stainless steel needles were used as the EHD nozzles due to their low cost and disposability. Their diameters and lengths are shown in Tab. 1.

Table 1. Commercial stainless-steel nozzles and their sizes

Type	Inner-diameter	Outer-diameter	length
32G	0.10 mm	2.40 mm	6.5/13 mm
30G	0.15 mm	0.30 mm	6.5/13 mm
28G	0.17 mm	0.32 mm	6.5/13 mm
27G	0.2 mm	0.40 mm	6.5/13 mm
26G	0.22 mm	0.45 mm	6.5/13 mm
25G	0.25 mm	0.50 mm	6.5/13 mm
24G	0.27 mm	0.55 mm	6.5/13 mm
23G	0.30 mm	0.60 mm	6.5/13 mm
22G	0.40 mm	0.70 mm	6.5/13 mm
21G	0.50 mm	0.80 mm	6.5/13 mm
20G	0.60 mm	0.90 mm	6.5/13 mm

Figure 2 presents the schematic diagram of the home-made pulsed-voltage EHD printing system for PZT droplet ejection. The system's core components and their functions are as follows: (1) Voltage control module: A DC high-voltage source (0-6 kV) provides the base voltage, which is modulated by a computer-controlled MOSFET pulse control board to generate pulsed voltage; this pulsed voltage is transmitted to the stainless-steel nozzle (Tab. 1 lists nozzle specifications) to establish an electric field between the nozzle and the grounded Ti-coated substrate. (2) Ink delivery module: A syringe pump (LSP02-2A, Longerpump, UK) is directly connected to the nozzle to supply PZT ink for EHD printing. (3) Motion and observation module: A computer sends position commands to the motion controller, which drives the X-Y stage (PH554-B2, VEXTA, Japan) to move the substrate and form desired patterns; a high-resolution camera (aligned to the nozzle tip) captures real-time images of the ink meniscus and printed droplets, with data fed back to the computer for process monitoring. All components are integrated to ensure stable control of pulsed voltage, ink flow, and substrate positioning, critical for reproducible PZT droplet ejection and microstructure printing.

The PZT precursor solution (serving as the matrix for subsequent ink formulation) was synthesized via a controlled sol-gel route, with all raw material amounts standardized to molar/mass/volume ratios (based on the target precursor volume of 100 mL) for reproducibility. The detailed, ratio-matched procedure is shown in Fig. 3 and described below.

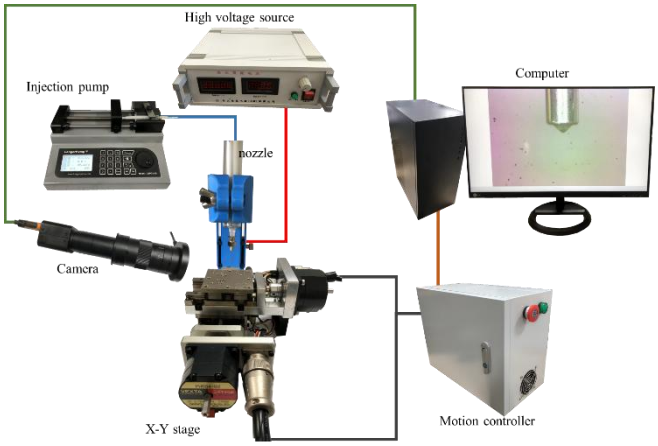

Fig. 2. Homemade EHD printing equipment

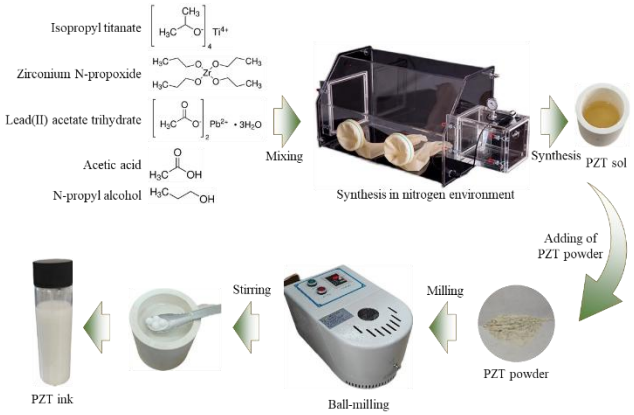

Fig. 3. The synthesis process of PZT ink used for EHD printing

(1) Initial precursor mixing (room temperature): First, acetylacetone ($C_5H_8O_2$, purity ≥ 99%, Sinopharm Chemical Reagent) and tetrabutyl titanate ($C_{16}H_{36}O_4Ti$, purity ≥ 98%, Aladdin Scientific) were mixed in a volume ratio of 3:5.6. The mixture was added to a 250 mL three-necked flask equipped with a magnetic stirrer, and stirred at 300 rpm for 5 minutes to ensure preliminary homo-geneity.

(2) Heated homogenization: The flask was placed in an oil bath, and the temperature was raised to 60 °C (controlled within ±1 °C). Magnetic stirring was maintained at 400 rpm for 60 minutes. This step promotes intermolecular interaction between acetylacetone and tetrabutyl titanate, forming a stable chelate complex to suppress premature hydrolysis.

(3) Ethylene glycol methyl ether addition (60 °C): Ethylene glycol methyl ether ($C_3H_8O_2$, purity ≥ 99%, Sinopharm Chemical Reagent) was added to the above complex at a volume ratio of 10:8.6. Stirring (400 rpm) was continued at 60 °C for 30 minutes until the solution became clear.

(4) Incorporation of zirconium and lead sources (60 °C):
Zirconium nitrate hexahydrate ($Zr(NO_3)_4·6H_2O$, purity ≥ 99%, Aladdin Scientific) and lead acetate trihydrate ($(Pb(C_2H_3O_2)_2·3H_2O$, purity ≥ 99%, Aladdin Scientific) were added sequentially in a mass ratio of 1:2.02. For 100 mL final solution, this translates to 6.9 g zirconium nitrate and 13.9 g lead acetate. Both reagents were added in small portions (5-10% of total mass per addition) to avoid agglomeration, while stirring at 500 rpm was maintained at 60 °C for 45 minutes until complete dissolution.

(5) Secondary solvent addition and high-temperature reaction: Additional ethylene glycol methyl ether was added at a volume ratio of 28:8.6. The oil bath temperature was raised to 90 °C (±1 °C), and stirring was adjusted to 450 rpm for 60 minutes. During this stage, the solution gradually turned orange-red (indicating complete dissolution of metal precursors and formation of PZT precursor complexes).

(6) Formamide modification (60 °C): Formamide (CH_3NO, purity ≥ 99%, Aladdin Scientific) was added at a volume ratio of 3:8.6. The oil bath temperature was lowered to 60 °C, and stirring (400 rpm) was continued for 60 minutes to allow formamide to act as a stabilizer, preventing precursor precipitation.

(7) Acetic acid adjustment (50 °C): Glacial acetic acid (CH_3COOH, 36% concentration, Aladdin Scientific) was added at a volume ratio of 20:8.6. The oil bath temperature was further lowered to 50 °C, and stirring (350 rpm) was maintained for 60 minutes to adjust the solution viscosity and pH (final pH: ~4.0).

(8) Filtration and quality control: The resulting solution was cooled to room temperature (~25 °C) and filtered through a 0.22 μm pore-size organic phase filter membrane to remove any undissolved impurities. The qualified precursor solution was clear and transparent with a pale yellow color. This appearance indicates no hydrolysis byproducts and confirms suitability for subsequent ink formulation.

(9) Cleaning of tetrabutyl titanate-contaminated reagents: Reagent bottles or flasks in contact with tetrabutyl titanate were cleaned sequentially with ethanol (C_2H_5OH, 95% concentration) for 30 minutes (to dissolve residual titanate) and deionized water (resistivity ≥ 18.2 MΩ·cm) for 20 minutes, followed by drying at 80 °C for 1 h to avoid cross-contamination in subsequent experiments.

The Ti substrate was directly used as the bottom electrode for PZT polarization and performance testing. After EHD printing of PZT structures, sintering (700 °C for 2 hours) and upper silver electrode deposition were conducted, followed by polarization via a home-made platform. The Ti substrate's conductivity ensures

effective electric field formation during EHD printing and reliable electrode function for the final PZT sensors.

The prepared PZT ink was deposited onto a titanium substrate via EHD printing to form desired structures (e.g., dots, lines, or membranes). Notably, the Ti substrate served directly as the bottom electrode for subsequent PZT polarization and performance characterization. The printed PZT structures were sintered at 700 °C for approximately 2 hours. After depositing the top silver electrode, the PZT structures were polarized using a home-built polarization platform (Fig. 4). This platform is equipped with a CCD camera and an XYZ stage for alignment, a sample holder for applying high voltage, and a heating bath for silicone oil temperature control. Following polarization, the PZT sensors were successfully fabricated.

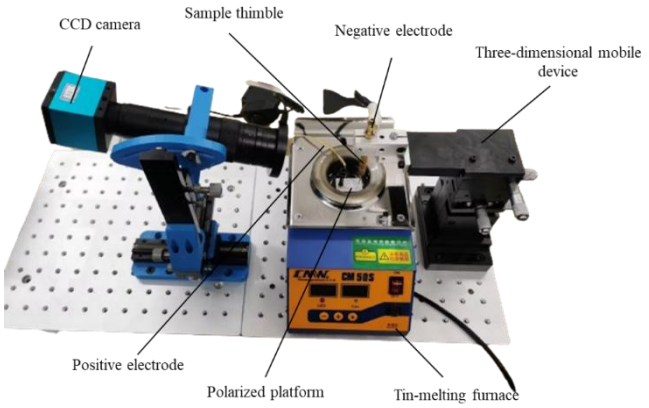

Fig. 4. Home-made PZT polarizing platform

3 Result and discussion

3.1 Numerical simulation of EHD printing process

3.1.1 Formation process of PZT droplets

The ink in the nozzle can be ejected under high voltage, which is an electrohydrodynamic phenomenon. The jet flow could be ejected under DC voltage, while droplets could be ejected under AC voltage. Previously, researchers have analyzed the formation of EHD jets under DC voltage. However, the formation of EHD droplets has rarely been systematically investigated via numerical simulation [26-28]. In the present work, we only studied the formation process of the droplets under AC voltage (pulsed voltage).

Droplets can form under dripping and EHD jet modes when suitable voltage and additional pressure are applied to the ink. The formation of droplets was investigated by numerical simulation in this work. Figures 5a to 5d show the ejection of a droplet under dripping mode. This mode could only occur at high ink pressure or ink flow rate. When a relatively high pressure is applied to the ink, the ink inside the nozzle is squeezed out (Fig. 5a). Due to the gravity and ink pressure, the squeezed ink begins to neck down and a spherical droplet forms (Fig. 5b). Restricted by the surface tension of the ink, a spherical droplet is finally ejected as shown in Figs. 5c and 5d. It is noticed that ink pressure is the primary factor for the formation of the droplet, rather than the applied voltage. Even without applying an electric voltage, droplets can still form at an appropriate ink pressure or flow rate. The diameter of the droplet is close to the inner diameter of the nozzle at dripping mode. Figures 5e-h show the generation of a droplet under EHD jet mode. The formation of EHD droplets can be explained as follows. There are lots of free charges in the ink [29]. When a bias voltage (tens to hundreds of volts) is applied to the ink, free charges within the ink migrate under the influence of the electric field and accumulate near the nozzle tip. Driven by the electric field force, the ink forms a meniscus at the nozzle tip (Fig. 5e). Upon application of the pulsed voltage, the electric field force is sufficiently strong to overcome the ink's surface tension, resulting in the ejection of a jet from the center of the meniscus (Fig. 5f). As the pulsed voltage is terminated, the sharpened meniscus retracts (Fig. 5g). Concurrently, the ejected jet breaks up. Subsequently, the fragmented jet segments contract under the action of surface tension, eventually coalescing into spherical droplets (Fig. 5h). For the EHD jet mode, the formation of EHD droplets is dependent on the applied pulsed voltage. In this mode, only an extremely low pressure (or ink flow rate) is imposed on the ink. Compared with the dripping mode, the EHD jet mode enables the generation of significantly smaller droplets, a key advantage for fabricating high-resolution microstructures.

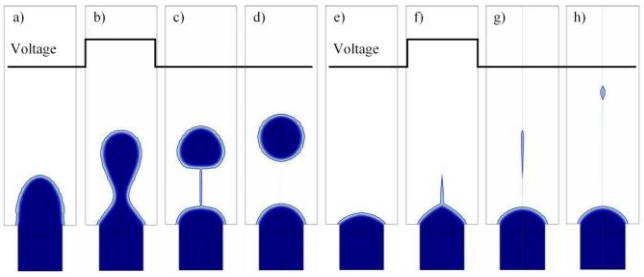

Fig. 5. Formation of droplets at dripping and EHD jetting modes, a)-d) show the dripping mode, while e)-h) show the EHD jetting mode.

The duration of the pulsed voltage exerts a significant influence on the formation of EHD droplets. When an inappropriate pulsed voltage is applied, multiple droplets may be ejected from the nozzle; these unwanted droplets are referred to as "satellite droplets". Notably, satellite droplets are prone to form under conditions of prolonged pulsed voltage duration. Figure 6 presents the

numerical simulation results illustrating the formation process of satellite droplets. The pulsed voltage parameters used here are identical to those in Fig. 5, with the only difference being the pulsed voltage duration, which is twice as long as that in Fig. 5.

As the pulsed voltage is applied, an EHD jet is initiated. Owing to the prolonged pulsed voltage duration, an extended EHD jet is generated even after the pulsed voltage is terminated, as depicted in Fig. 6c. Due to the excessive length of the ejected jet and the velocity discrepancy along the jet axis, the trailing segment of the ink cannot keep pace with the leading segment. Driven by surface tension, the jet subsequently breaks into two separate droplets (Figs. 6d and 6e), with the smaller secondary droplet being the satellite droplet.

Satellite droplets undermine the printing precision of the target microstructures, making their suppression critical for high-quality EHD printing. Our simulation results confirm that the duration of the pulsed voltage is a key factor governing satellite droplet formation: to avoid satellite droplets, the pulsed voltage duration must be constrained within a specific optimal range; exceeding this range will lead to the generation of satellite droplets.

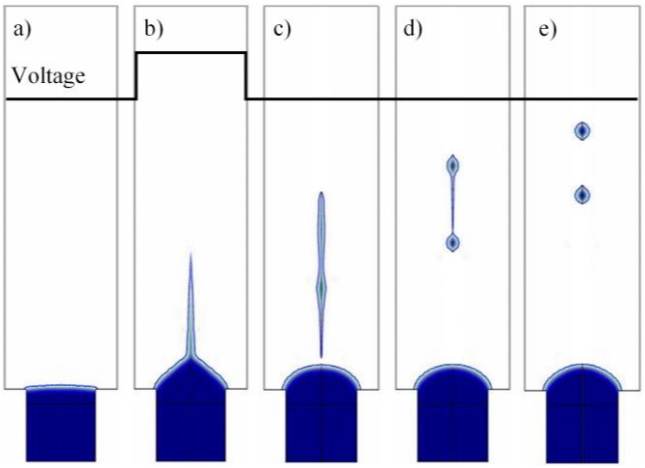

Fig. 6. The formation of satellite droplet

3.1.2 The influence of printing parameters on the size of ejected droplets

There are four factors that could influence the size of ejected droplets. They are voltage amplitude, duty ratio of the voltage, printing distance, and flow rate/ink pressure. The voltage amplitude and printing distance are the only two parameters that directly influence the electric field strength: increasing the voltage amplitude or decreasing the printing distance enhances the electric field, which in turn affects the droplet ejection behavior. Therefore, we only investigated its voltage amplitude dependence.

Figure 7a illustrates the effect of voltage amplitude (Volt) on the radius of ejected droplets, with the tested voltage amplitude spanning 1000-5000 V. Figure 7a reveals a negative correlation between voltage amplitude and droplet radius: a larger droplet radius is associated with a lower voltage amplitude. This trend aligns with the behavior of direct current (DC) voltage-based EHD printing reported in our previous study [24], confirming that droplet radius decreases as voltage amplitude increases. Figure 7b, in turn, depicts the relationship between the duty ratio (DR) of the applied pulsed voltage and ejected droplet radius. Here, the duty ratio is defined as the ratio of the pulsed voltage duration to the total voltage cycle duration – a key parameter governing the effective duration of electric field action on the ink. We found that when the duty ratio is lower than 0.15, EHD droplets cannot form, while when it exceeds 0.5, the ejected droplets become excessively large (hundreds of micrometers). Thus, the chosen duty ratio ranges from 0.15 to 0.5. From Fig. 7b, it is obvious that larger droplets are associated with a higher duty ratio. A high duty ratio corresponds to a longer EHD jetting duration, resulting in the ejection of a large volume of ink from the nozzle and thus an increase in droplet radius. Droplet radius increases with the duty ratio within the range of 0.15-0.5. Figure 7c shows the influence of flow rate (FR) on the radius of the droplets. The flow rate ranges from 0.07 to 0.1 m/s. Similar to the duty ratio, a high flow rate leads to a large volume of ejected ink. Then the radius of the droplet increases. The radius is in direct proportion to the flow rate. Droplet radius shows a positive correlation with the ink flow rate (0.07-0.1 m/s). Figure 7d shows the influence of printing distance (PD, the distance between the nozzle tip and the substrate) on the radius of the droplets. Droplet radius increases as the printing distance increases. Figure 7e shows the effect of inner diameter (ID) on the radius of the droplets. Droplet radius is positively correlated with the inner diameter of the nozzle. Finally, Pearson correlation analysis was performed by SPSS (version 27, IBM, USA) to evaluate the strength of linear relationships between printing parameters and the radius of ejected droplets. The Pearson correlation coefficient (r) is the most common way of measuring a linear correlation, ranging from –1 to 1. Pearson correlation analysis (Fig. 7f) quantifies the linear relationships between printing parameters and droplet radius: the duty ratio exhibits the strongest positive correlation (r=0.86), followed by flow rate (r=0.24) and printing distance (r=0.27), while the inner diameter shows the weakest positive correlation (r=0.08). Notably, voltage amplitude presents a weak negative correlation (r=–0.38). This indicates that most printing parameters contribute to larger droplet radii when enhanced: duty ratio, where longer pulse duration leads to more ink ejection; flow rate, where higher volume supply results in larger droplet formation; printing distance, where longer distance induces

extended jet length and thus increased droplet volume; and inner diameter, where a larger nozzle facilitates more ink output. In contrast, higher voltage amplitude unexpectedly reduces droplet radius, which is likely attributed to the transition of jet mode under pulsed AC voltage: when voltage exceeds a critical threshold (~3 kV in this study), the stable cone-jet mode shifts to a mild multi-jet mode, where the ejected ink splits into smaller sub-jets, ultimately reducing the average radius of individual droplets.

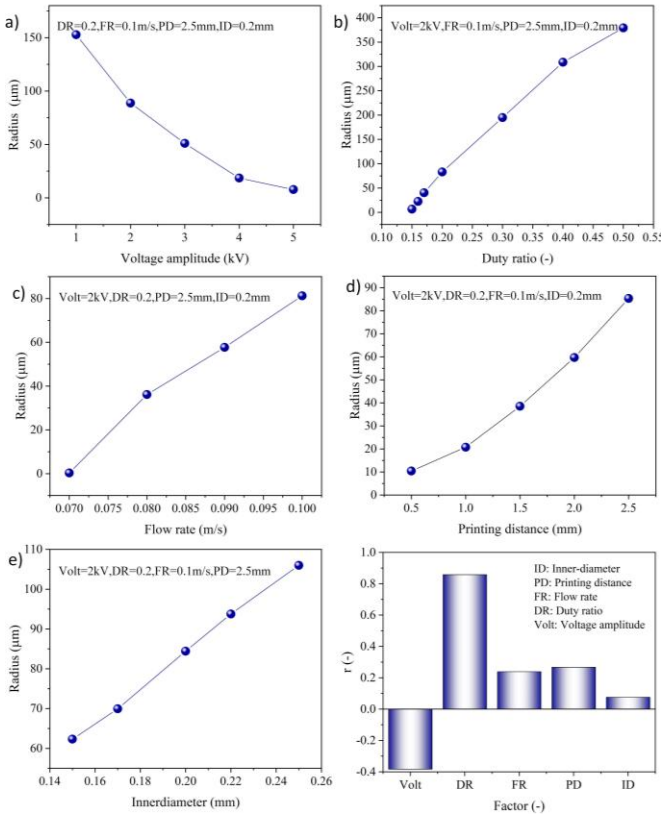

Fig. 7. The effect of printing parameters on the size of ejected droplets, the influence of a) voltage amplitude, b) duty ratio, c) flow rate, d) printing distance, and e) inner diameter on the radius of the ejected droplets, f) Pearson correlation coefficients indicating the strength of relationships between printing parameters and the radius of ejected droplet.

3.1.3 The relationship between the physical properties of the ink and the size of ejected droplets

The formation of droplets can be affected by the physical properties of the ink, including conductivity, density, permittivity, surface tension coefficient, and viscosity. These properties can be adjusted by changing the ink concentration or solvent composition. Figure 8 shows the effect of ink physical properties on the size of the ejected droplet. The conductivity is the only factor that hardly affects the droplet radius (Fig. 8a). The density and viscosity are the factors which have a nearly linear relationship with the droplet radius. A larger droplet radius is associated with lower ink density and viscosity (Fig. 8b and c), meaning droplet radius de-creases as ink density or viscosity increases – consistent with the negative correlation between viscosity and droplet radius. A larger droplet radius correlates to higher permittivity. The radius is in direct proportion to ink permittivity (Fig. 8d).

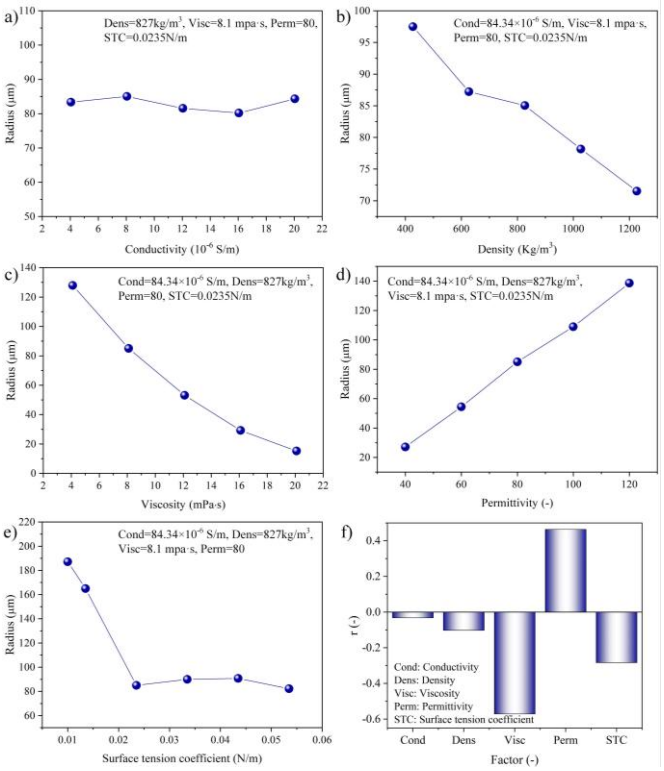

Fig. 8. Relationship between the physical properties of the ink and the radius of ejected droplets, the influence of a) conductivity, b) density, c) viscosity, d) permittivity, and e) surface tension coefficient on the radius of the ejected droplets, f) Pearson correlation coefficients indicating the strength of relationships between ink physical properties and the radius of ejected droplet.

Droplet radius increases proportionally with ink permittivity. The droplet radius drops when the surface tension coefficient increases from 0.01 to 0.024 N/m (Fig. 8e), as higher surface tension resists the electric field-induced jetting. However, when the surface tension coefficient continues to increase beyond 0.024 N/m (up to 0.06 N/m in this study), the electric field force is no longer able to significantly deform the ink meniscus, leading to nearly unchanged droplet radius. When the electric field force overcomes the surface tension of the ink, EHD jet flow could eject from the nozzle. A small surface tension coefficient enables the electric field force to easily overcome the liquid-gas interface tension under

a constant applied voltage, resulting in a larger volume of ejected droplets. When the surface tension increases to a threshold value, the ink could be well held inside the nozzle, which might cause the nearly unchanged radius of ejected droplets. Figure 8f shows the calculated Pearson correlation coefficient (r). Pearson correlation analysis (Fig. 8f) reveals the direction and strength of relationships between ink physical properties and droplet radius: viscosity exhibits the strongest correlation (r=–0.57), followed by permittivity (r=0.46) and surface tension coefficient (r =–0.28), while density shows a weak negative correlation (r=–0.1), and conductivity has the weakest correlation (r=–0.03, nearly no linear influence). The negative r values for viscosity, density, and surface tension coefficient indicate that increasing these properties reduces droplet radius – physically, higher viscosity/density inhibits ink flow, and higher surface tension resists electric field-induced jetting, thereby reducing ejected droplet volume.

3.1.4 Calculation of the conditions for a printed droplet with desired radius

Based on the simulation results, the printing parameters and ink physical properties can be optimized to achieve the ejection of droplets with the target size. In this study, the calculation model focused on droplet radii ranging from 1 to 100 μm. The radar charts in Fig. 9 are based on the simulation data from Figs. 7 and 8, which reflect the quantitative relationships between printing parameters, ink physical properties, and droplet radius. To standardize the indices on the radar chart axes, all printing parameters and ink physical properties were normalized with respect to their maximum values. The data in Fig. 9 are derived from simulations of the droplet radius dependence on printing parameters and ink physical properties. This approach enables prediction of suitable printing parameters and ink physical properties for fabricating droplets with radii in the 1-100 μm range, which is critical for meeting the microstructural requirements of MEMS PZT sensors.

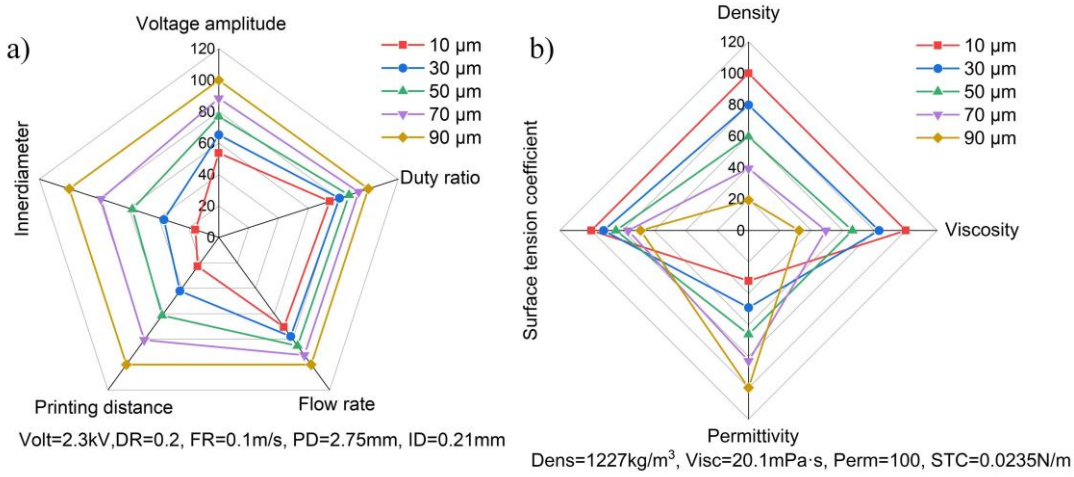

Fig. 9. Radar maps for a) printing parameters (voltage amplitude, duty ratio, flow rate, printing distance, inner diameter), and b) ink physical properties (density, viscosity, permittivity, surface tension coefficient, conductivity)

3.2 Experimental investigation of PZT EHD printing

The radar charts obtained by numerical simulation can serve as a reference for selecting suitable printing parameters and physical properties of PZT inks, and the printed PZT size could also be estimated by the radar maps. Subsequently, PZT EHD printing was performed by using pulsed high voltage. Figure 10 shows the formation of the PZT EHD jet under pulsed voltage. The voltage contains bias voltage V_{bias} and pulse voltage V_{pulse}. The bias voltage is used to maintain the Taylor cone, while the pulse voltage is used to form the jet ejected from the Taylor cone. One can see that the PZT jet is ejected from the nozzle after applying the pulse voltage, while the PZT jet stops when the voltage returns to the bias voltage.

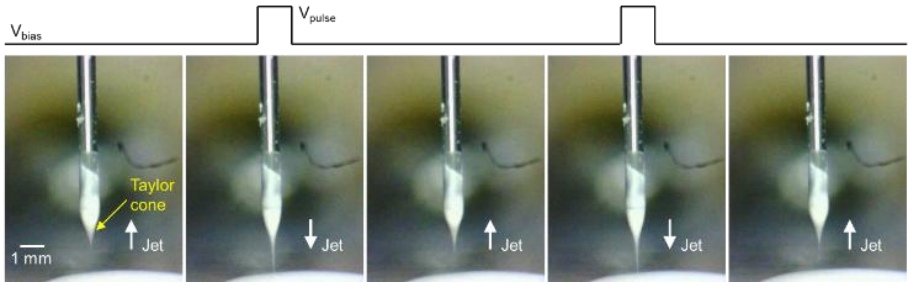

Fig. 10. The formation of EHD jet under pulsed voltage

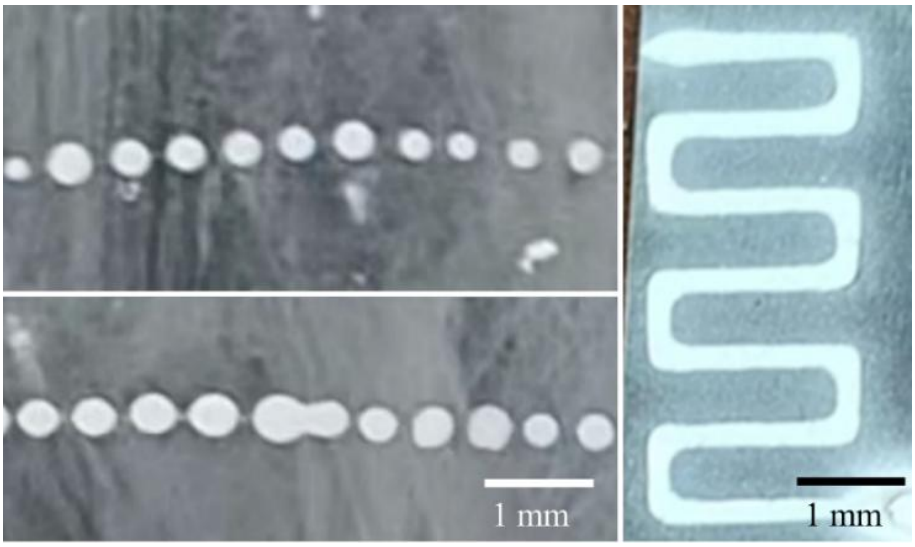

Fig. 11. The fabricated PZT dots and lines by EHD printing

Both PZT dots and lines were successfully deposited onto Ti substrates by adjusting the printing speed. When the printing speed is higher than the PZT ejecting speed, PZT dots can form (Fig. 11a). As the printing speed is much lower than the PZT ejecting speed, PZT lines can be printed due to the overlap of printed PZT dots (Fig. 11b).

Via EHD printing, desired PZT microstructures were successfully deposited onto Ti substrates. Post-printing, the PZT structures required sintering to enhance their crystallinity and mechanical stability; in this study, sintering was performed at 700 °C for 2 hours. Figures 12a and 12b present scanning electron microscopy (SEM) images of the PZT structures before and after sintering, respectively. It is evident from these images that PZT particles undergo fusion after sintering, confirming the densification of the printed structure. Additionally, the images demonstrate the uniform dispersion of PZT powder within the sol-gel matrix and the smooth surface morphology of the as-printed PZT – key characteristics for ensuring consistent piezoelectric performance.

Figure 12c shows the X-ray diffraction pattern of the sintered PZT films. A prominent diffraction peak corresponding to the PZT (110) plane is observed, indicating a strong preferential orientation. Other characteristic diffraction peaks of PZT, including (100), (111), (200), (210), (211), and (202), are also detected, which are consistent with the standard diffraction profile of perovskite PZT. No secondary-phase peaks are visible in the XRD pattern, confirming the high purity of the crystalline PZT structure formed during the annealing process – this purity is critical for maintaining excellent piezoelectric sensitivity.

To validate the feasibility of the proposed EHD printing method for PZT sensor fabrication, a PZT layer was printed onto a Ti cantilever (200 μm in width, inset of Fig. 12d). The Ti cantilever was prefabricated via laser cutting. The EHD-printed PZT layer was first sintered at 700 °C for 2 h and subsequently polarized at 2000 V for 15 minutes. For sensor assembly, the Ti cantilever served as the bottom electrode, while a sputtered silver (Ag) layer on the PZT surface acted as the top electrode.

Figure 12d presents the performance test results of two fabricated PZT cantilever sensors: one with polarization treatment and one without. The sensors were tested by applying airflow (via manual air blowing) to induce mechanical vibration. The unpolarized PZT sensor exhibited negligible response to airflow changes, even under strong blowing (red curve in Fig. 12d). In contrast, the polarized PZT sensor demonstrated a highly sensitive response to airflow variations, with distinct signal fluctuations (black curve in Fig. 12d). These experimental results, combined with the consistency between simulation predictions and practical printing outcomes, confirm that the EHD-printed PZT structures possess excellent piezoelectric functionality after proper sintering and polarization – highlighting the great potential of the proposed method for manufacturing high-performance PZT sensors and miniaturized MEMS devices.

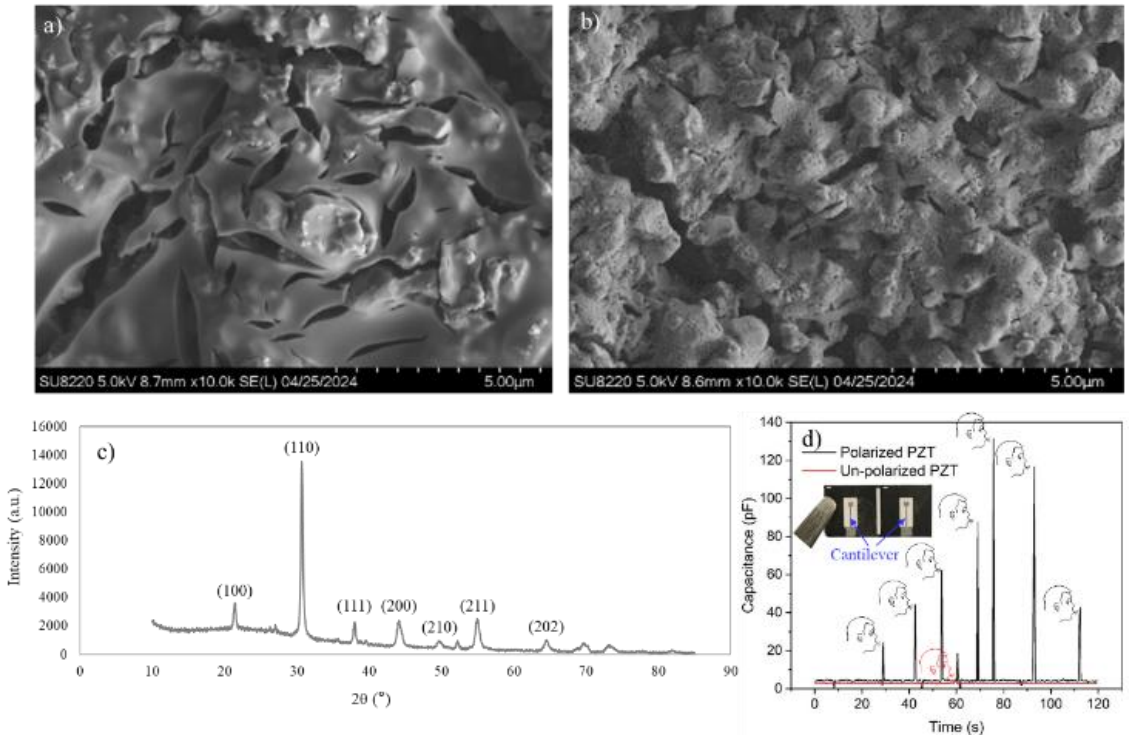

Fig. 12. The fabricated PZT structures by EHD printing, a) The SEM images of PZT before sintering, b) The SEM images of PZT after sintering under temperature of 700 °C for 2 h, c) The XRD image of sintered PZT, d) The test of PZT cantilevers

4 Conclusion

In this study, a numerical simulation method was developed to analyze the formation mechanism of electrohydrodynamic (EHD) droplets under high-voltage pulses. Specifically, the process of EHD droplet generation was systematically investigated, and the effects of printing parameters and ink physical properties on the radius of ejected droplets were quantified. Simulation results reveal that the duty ratio of the pulsed voltage is a critical factor governing droplet uniformity: an excessively large duty ratio promotes the generation of satellite droplets, which degrade printing precision. Additionally, droplet size exhibits clear correlations with key variables: larger droplets are associated with higher voltage amplitude, higher duty ratio, higher ink flow rate, and higher ink permittivity. In contrast, lower ink viscosity, lower ink density, and lower surface tension coefficient lead to smaller droplet sizes. Using the optimized printing parameters derived from simulations, PZT sol-gel is successfully deposited onto titanium (Ti) substrates to form target microstructures, including discrete dots and serpentine lines. The consistency between simulation predictions and experimental results, combined with the excellent piezoelectric performance of the fabricated sensors, demonstrates that the proposed method exhibits significant potential for the manufacturing of high-performance PZT-based sensors and miniaturized micro-electro-mechanical systems (MEMS) devices.

Acknowledgments

This project is supported by the open fund from Anhui Province Key Laboratory of Advanced Numerical Control & Servo Technology (XJSK202509), State Key Laboratory of Water Pollution Control and Green Resource Recycling (PCRRF25037), State Key Laboratory of Refractories and Metallurgy (G202202), Guangxi Key Laboratory of Automatic Detecting Technology and Instruments (YQ22208).

References

[1] Q.C. Zhang, X. Wang, Z.Y. Mao, A.B. Yang, S.Z. Niu, W. Gao and M. Wang, "Ferroelectric lead zirconate titanate-modified separator enabling stable anode-free lithium metal batteries via dual regulation of Li plus flux and anion-enriched solid electrolyte interphase", *Journal of Colloid and Interface Science*, vol.703, no. pp. 139195, 2026

[2] K. Cao, Q.C. Zheng, H. Chen, B. Xie, N. Deng, H. Shang, Y. Lu and H.K. Xie, "A tip-tilt-piston piezoelectric micromirror with double-S shaped actuators based on sputtered PZT", *Sensors and Actuators a-Physical*, vol.391, no. pp. 116666, 2025

[3] W.G. Lee and Y.J. Kwon, "Preparation of ferroelectric PZT thin films by plasma enhanced chemical vapor deposition using metalorganic precursors", *Journal of Industrial and Engineering Chemistry*, vol.14, no. 1, pp. 89-93, 2008

[4] D.M. Ai, D.L. Zhang and H.P. Zhu, "A damage localization approach for concrete structure using discrete wavelet transform of electromechanical admittance of bonded PZT transducers", *Mechanical Systems and Signal Processing*, vol.218, no. pp. 111531, 2024

[5] V.C. Nguyen, M.Q. Le, A. Fimbel, S. Bernadet, Y. Hebrard, J.F. Mogniotte, J.F. Capsal and P.J. Cottinet, "Evaluation of electromechanical characteristics for screen printed piezoelectric sensor-based Pu/PZT composite". *Electroactive Polymer Actuators and Devices (Eapad) Xxiv*, Long Beach, USA, vol.12042, no., pp. 120420X, 2022.

[6] K. Li, L. Sun, X.C. Yang, C. Wang, M.Z. Li, Z.J. Qiao and D.B. Ruan, "3D printing piezoelectric nanostructures via synergistic electrohydrodynamic and in-situ electrodeformation for highly sensitive sensing", *Chemical Engineering Journal*, vol.519, no. pp. 165333, 2025

[7] K. Li, Y.X. Wang, M.Z. Li, J.B. Li, F. Du, C. Wang, J.Y. Fang, L. Sun and X.Y. Wang, "3D printed ultrahigh aspect ratio lead zirconate titanate (PZT) nanostructures for nano-Newton force sensing", *Journal of the European Ceramic Society*, vol.44, no. 7, pp. 4646-4656, 2024

[8] H.T. Qin, J.Y. Dong and Y.S. Lee, "AC-pulse modulated electrohydrodynamic jet printing and electroless copper deposition for conductive microscale patterning on flexible insulating substrates", *Robotics and Computer-Integrated Manufacturing*, vol.43, no. pp. 179-187, 2017

[9] O. Yogi, T. Kawakami, M. Yamauchi, J.Y. Ye and M. Ishikawa, "On-demand droplet spotter for preparing pico-to femtoliter droplets on surfaces", *Analytical Chemistry*, vol.73, no. 8, pp. 1896-1902, 2001

[10] Y. Huang, N. Bu, Y. Duan, Y. Pan, H. Liu, Z. Yin and Y. Xiong, "Electrohydrodynamic direct-writing", *Nanoscale*, vol.5, no. 24, pp. 12007-12017, 2013

[11] S.-Y. Kim, K. Kim, Y. Hwang, J. Park, J. Jang, Y. Nam, Y. Kang, M. Kim, H. Park and Z. Lee, "High-resolution electrohydrodynamic inkjet printing of stretchable metal oxide semiconductor transistors with high performance", *Nanoscale*, vol.8, no. 39, pp. 17113-17121, 2016

[12] Y. Wu, B. Wu, S. Vijayavenkataraman, Y. San Wong and J.Y.H. Fuh, "Crimped fiber with controllable patterns fabricated via electrohydrodynamic jet printing", *Materials & Design*, vol.131, no. pp. 384-393, 2017

[13] K. Li, F. Du, J.Y. Fang, L. Sun, M.Z. Li, Y.X. Wang, C. Wang, X.Y. Wang, J.B. Li, Z.J. Qiao and D.B. Ruan, "Printed bioinspired piezoelectric nano-hair for ultrahigh sensitive airflow detection", *Chemical Engineering Journal*, vol.490, no. pp. 151570, 2024

[14] K. Li, S.F. Fan, X.Y. Wang and Y. Lu, "3D nanoprinting piezoceramic with large elastic deformation and high piezoelectricity", *International Journal of Extreme Manufacturing*, vol.7, no. 4, pp. 045006, 2025

[15] D. Wang, W. Zha, L. Feng, Q. Ma, X. Liu, N. Yang, Z. Xu, X. Zhao, J. Liang and T. Ren, "Electrohydrodynamic jet printing and a preliminary electrochemistry test of graphene micro-scale electrodes", *Journal of Micromechanics and Microengineering*, vol.26, no. 4, pp. 045010, 2016

[16] A. Ganan-Calvo, J. Davila and A. Barrero, "Current and droplet size in the electrospraying of liquids. Scaling laws", *Journal of Aerosol Science*, vol.28, no. 2, pp. 249-275, 1997

[17] J. Park, M. Hardy, S. Kang, K. Barton, K. Adair, D.K. Mukhopadhyay, C.Y. Lee, M.S. Strano, A.G. Alleyne, J.G. Georgiadis, P.M. Ferreira and J.A. Rogers, "High-resolution electrohydrodynamic jet printing", *Nature Materials*, vol.6, no. 10, pp. 782-789, 2007

[18] J. Li, "Formation and stabilization of an EHD jet from a nozzle with an inserted non-conductive fibre", *Journal of Aerosol Science*, vol.36, no. 3, pp. 373-386, 2005

[19] M. Paine, M. Alexander, K. Smith, M. Wang and J. Stark, "Controlled electrospray pulsation for deposition of femtoliter fluid droplets onto surfaces", *Journal of Aerosol Science*, vol.38, no. 3, pp. 315-324, 2007

[20] O. Lastow and W. Balachandran, "Numerical simulation of electrohydrodynamic (EHD) atomization", *Journal of Electrostatics*, vol.64, no. 12, pp. 850-859, 2006

[21] X. Wu, R.D. Oleschuk and N.M. Cann, "Characterization of microstructured fibre emitters: in pursuit of improved nano electrospray ionization performance", *Analyst*, vol.137, no. 18, pp. 4150-4161, 2012

[22] R.T. Collins, J.J. Jones, M.T. Harris and O.A. Basaran, "Electrohydrodynamic tip streaming and emission of charged drops from liquid cones", *Nature Physics*, vol.4, no. 2, pp. 149-154, 2008

[23] R.T. Collins, K. Sambath, M.T. Harris and O.A. Basaran, "Universal scaling laws for the disintegration of electrified drops", *Proceedings of the National Academy of Sciences of the United States of America*, vol.110, no. 13, pp. 4905-4910, 2013

[24] X. Yang, S. Wang, Z. Yin and W. Hu, "Numerical study on the electrohydrodynamic jet printing", *Journal of Micro and Nano-Manufacturing*, vol.9, no. 1, pp. 011001, 2021

[25] W. Wu, X. Yang, B. Zhang, Z. Yin and B. Jia, "The study on electric field distribution and droplet trajectory during electrohydrodynamic jet printing", *Microsystem Technologies*, vol.27, no. 7, pp. 2745-2750, 2021

[26] X. Yang, R. Liu, L. Li, Z. Yin, K. Chen and D.F. Wang, "The study of electrohydrodynamic printing by numerical simulation", *Journal of Electrical Engineering*, vol.71, no. 6, pp. 413-418, 2020

[27] Y. Pan and L. Zeng, "Simulation and Validation of Droplet Generation Process for Revealing Three Design Constraints in Electrohydrodynamic Jet Printing", *Micromachines*, vol.10, no. 2, pp. 94, 2019

[28] J.S. Lee, S.Y. Kim, Y.J. Kim, J. Park, Y. Kim, J. Hwang and Y.J. Kim, "Design and evaluation of a silicon based multi-nozzle for addressable jetting using a controlled flow rate in electrohydrodynamic jet printing", *Applied Physics Letters*, vol.93, no. 24, pp. 243114, 2008

[29] J.R. Melcher and G.I. Taylor, "Electrohydrodynamics: A Review of the Role of Interfacial Shear Stresses", *Annual Review of Fluid Mechanics*, vol.1, no. 1, pp. 111-146, 1969

Xue Yang received her PhD degree in Mechanical Engineering from Jilin University, Changchun, China, in 2024. In September 2016, she joined the School of Civil Engineering, Jilin Jianzhu University, Changchun, China. Her research interests include MEMS technology and 3D printing technology.

Mingchao Bi received her PhD degree from Jilin University, Changchun, China, with one year of academic study experience in the United States. Currently, she holds the positions of Young and Middle-aged Editorial Board Member at the national-level journal Eye Science, Youth Committee Member of the Chinese Women Ophthalmologists Association, and Youth Committee Member of the Neuro-Ophthalmology Professional Committee of the Chinese Research Hospital Association. To date, she has published 15 academic papers and 16 conference papers.

Zhifu Yin received his PhD degree in Mechanical Engineering from Dalian University of Technology, Dalian, P. R. China, in 2016. He received postdoctoral training at the California Institute of Technology in 2021. In June 2016, he joined the School of Mechanical and Aerospace Engineering, Jilin University, Changchun, China. His research interests include MEMS/NEMS technology, 3D printing, and micro/nanofluidic systems. He has published more than 80 research articles in the fields of MEMS and micro/nanofluidic devices.

Received 12 September 2025